journal

J. Am. Ceram. Soc., **86** [9] 1578–85 (2003)

Formation of β-Silicon Nitride Crystals from (Si,Al,Mg,Y)(O,N) Liquid: I, Phase, Composition, and Shape Evolutions

Lingling Wang* and Tseng-Ying Tien*

Department of Materials Science and Engineering, University of Michigan, Ann Arbor, Michigan 48109-2136

I-Wei Chen*

Department of Materials Science and Engineering, University of Pennsylvania, Philadelphia, Pennsylvania 19104-6272

Precipitation, growth, and coarsening of Si_3N_4 crystals in (Si,Al,Mg,Y)(O,N) liquids at 1680°C has been studied. The initial nucleation of β-Si_3N_4 occurs mostly on α-Si_3N_4 because of the very high supersaturation of the liquid. After a brief period of growth, the crystals then undergo accelerated coarsening, decreasing the crystal concentration by almost 100 times with little change in the total crystal volume. Meanwhile, the crystals gradually transform from β-Si_3N_4, by substituting Si-N with Al-O, to β′-SiAlON of various compositions. The evolution of aspect ratio strongly depends on the Si/(Al,Mg,Y) ratio, which is rationalized by cation segregation to the interface driven by the acidity–basicity differential between the liquid and the crystal.

I. Introduction

THE precipitation, growth, and coarsening of hexagonal rodlike crystals from supersaturated liquid is a rather common phenomenon in nature. Its occurrence in ceramic processing, especially in silicon nitride (Si_3N_4) systems, has attracted much attention.[1–5] This is because such rodlike crystals often result in interlocking microstructures that can impart greatly enhanced resistance to crack propagation in otherwise brittle ceramics.[6,7] As a result, tough ceramics with properties similar to those of whisker-reinforced materials can be achieved. Engineering ceramics based on Si_3N_4 as well as several glass-ceramic formulations are the direct consequence of such microstructures. An understanding of the nucleation, growth, and coarsening of rodlike crystals is therefore of considerable importance.

Extensive data of crystal growth in Si_3N_4 ceramics have been reported by Hwang and co-workers[1,2] and Lai and Tien,[3] among others. Their data, however, are strongly influenced by crystal impingement because of the high volume fraction (typically >85%) of crystals in such ceramics. Therefore, a direct comparison of their observations with theoretical, kinetic models is problematic.[8–10] Moreover, crystal dimensions in ceramics are difficult to ascertain from planar cross sections, which were used in the Hwang *et al.* study. Indeed, even if effort is made to extract crystals from the ceramics, as in the Lai *et al.* study, the extracted crystals may not share the same sampling statistics as those in the ceramics. These difficulties led Krämer *et al.*[4,5] to investigate crystal growth of samples that contain a much smaller fraction of Si_3N_4 crystal (~5%–10%). Their kinetic analysis,[4] however, appears to be limited to the initial stage of crystal growth, when the driving force primarily comes from the concomitant α-Si_3N_4 to β-Si_3N_4 transformation. Also, while they used a Y-Al-Si-O-N system, which undergoes precipitation of both β-Si_3N_4 and β′-SiAlON, the kinetic effect of these phases was not studied. In this study, we have investigated several other compositions and for a more extended kinetic range to explore the effects of composition, phase transformation, and driving force on crystal growth. Although the basic design of our experiments is similar to that of Krämer *et al.*, a higher temperature (1680°C) was used to examine a fuller range of kinetic evolution within 4 h. A new sampling technique was also used, which, we believe, provided rather accurate data of crystal dimensions.

Our results are presented in two parts. In this article (Part I), we describe the data that leads us to new insight into the phase nucleation and evolution as well as the effect of composition on crystal morphology in the Si_3N_4–SiAlON systems. In the second article (Part II), we describe the crystal population dynamics to determine the growth velocity and to make a comparison with the theoretical predictions of crystal growth and coarsening based on a recent theory.[11] A further examination and modeling of the shape transition at the ends of a rod-shaped crystal[12] are reported elsewhere using the dimensional and velocity data obtained here.

II. Experimental Procedure

(1) Compositions

The compositions investigated are shown in Table I. They are designed to have an approximately constant O/N ratio so that the liquid viscosity and, hence, kinetics are mostly comparable. They also have the same Al/Y/Mg ratio. The main difference is the Si/(Al,Y,Mg) ratio, which increases from CY1 to CY4. As discussed later, the amount of β-Si_3N_4/β′-SiAlON crystals that eventually precipitates from the liquid at the test temperature (1680°C) is ~15%. In our preliminary experiment, we have determined the (metastable) solubility of β-Si_3N_4 to be 11%–12%

Table I. Sample Composition, Equivalent Percent N/O Ratio, Equivalent Percent Cation Ratio, and Experimentally Measured β/β′ Fraction at the End of the Experiment

	Composition (mol)							
Sample	Si_3N_4	SiO_2	Al_2O_3	Y_2O_3	MgO	N/O	Si/(Al,Y,Mg)	β/β′ (vol %)
CY1	2.3	9.3	6.3	1.7	3.4	0.31	1.18	18 ± 2
CY2	2.4	10.2	6.3	1.7	3.4	0.30	1.27	16 ± 2
CY3	2.5	11.0	6.3	1.7	3.4	0.30	1.35	14 ± 2
CY4	2.5	11.9	6.3	1.7	3.4	0.30	1.42	13 ± 2

R. Riedel—contributing editor

Manuscript No. 186715. Received August 22, 2002; approved April 14, 2003.

Supported by the U.S. Department of Energy, under Contract No. DE-AC05–84OR22464, and by the Air Force Office of Scientific Research, under Grant No. AFOSR-G-F49620–01-1–0150. Facilities at the University of Pennsylvania are supported by the U.S. National Science Foundation under MRSEC Grant No. DMR00-79909.

*Member, American Ceramic Society.

(without crystallization) when the composition of SiO_2, Al_2O_3, Y_2O_3, and MgO is the same as CY1. The metastable solubility of β-Si_3N_4 is higher in CY2–CY4, but the accurate value has not been determined.

The starting powders used were Si_3N_4 (SN-E10, Ube Co., Tokyo, Japan), Y_2O_3 (99.99%, Aldrich Chemical Co., Milwaukee, WI), Al_2O_3 (AKP-50, Sumitomo Chemical Co., Osaka, Japan), $4MgCO_3{\cdot}Mg(OH)_2{\cdot}nH_2O$ (40.6% assay as MgO, J. T. Baker, New York), and SiO_2 (99.8% amorphous SiO_2, Sigma Chemical Co., New York). The Si_3N_4 powder had an α content >95.5% and contained 1.57 wt% oxygen, which was taken into account in the powder formulation.

(2) Powder Processing and Sintering

Appropriate amounts of powders were ball-milled with 2-propanol for 12 h using high-purity Si_3N_4 milling media. The mixtures were subsequently stirred and dried on a hot plate under an infrared lamp. After they were dried, the powder mixtures were sieved and cold-pressed into pellets. Pellets of all four compositions were placed in a BN-coated graphite crucible and sintered under 1.5 MPa nitrogen-gas for a specified time. The temperature was controlled to be 1680° ± 10°C. On reaching temperature, samples were held from 8 to 256 min before cooling. A constant heating rate of 24°C/min from 800° to 1680°C was used. Cooling was effected by turning off the furnace power, during which a cooling rate of ~1.5°C/s from 1680° to 1200°C was recorded.

(3) Characterization

Identification of crystalline phases was made using X-ray diffractometry (XRD) with Cu*K*α radiation. To estimate the composition of β′-SiAlON, the quantitative method of Ref. 13 was followed. Coarse-grained silicon powders were used as an internal XRD standard. Scanning electron microscopy (SEM; Model XL30FEG, Philips, Eindhoven, The Netherlands) was used for further phase identification and microstructure characterization. Phase identification using SEM was based on the assumption that α-Si_3N_4 has a rounded shape, whereas β-Si_3N_4 and β′-SiAlON have elongated shapes. To determine the area fraction of crystalline phases (α versus β/β′), polished samples were plasma etched and then viewed in the back-scattering electron mode. Figure 1(a) shows such an image, revealing the compositional contrast between Si_3N_4 crystals (dark) and the Y-Mg-Si-Al-O-N glass (bright). At least 20 images of ~100 μm^2 each were taken for the estimation of phase fractions.

Dimensions of β/β′ crystals were determined using SEM in the secondary electron mode. To aid measurement, polished samples were chemically etched using molten alkali hydroxides (NaOH and KOH in equal weight) at 500°C. The SEM images revealed the hexagonal rod shape of Si_3N_4 crystals (Fig. 1(b)). For quantitative analysis of dimensions, we excluded those crystals whose full length and width were not apparent from the micrographs. Thus, crystals with only one end visible but with the other end embedded in the glass were not considered. Likewise, crystals without at least two side surfaces fully exposed were excluded. The remaining crystals that were visible on the micrographs were counted, and, in total, 500 crystals were used to determine the length (L) and width (W) distributions in each sample. The above procedure ensured that all these crystals were almost parallel to the polished section, yet they represented an unbiased sampling of the entire crystal population in the bulk, because there was no texture in our samples.

In the above measurement, the width was taken as the spacing between the outer edges of either two or three adjacent side surfaces. These two measures differed by 14%, but we made no distinction between them. Therefore, the reported W value was essentially the statistical average of the two measures with an inherent uncertainty of 14%. Identifying W with the above average, we found the hexagonal cross-sectional area was $0.75W^2$, which was numerically similar to $\pi W^2/4$. Thus, the W value reported might also be regarded as the diameter of an equivalent circle that has the same area as the cross section of the hexagonal rod.

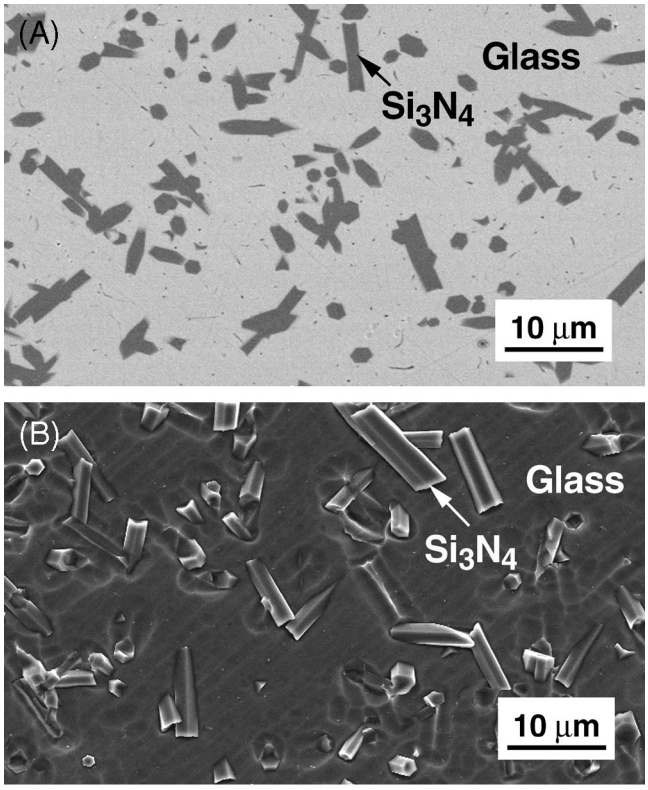

Fig. 1. (a) Back-scattering electron image of polished section, plasma etched (CY3 after 256 min at 1680°C). (b) Secondary electron image of polished section, NaOH:KOH melt etched (CY3 after 256 min).

III. Results

(1) Phase Analysis

Phase analysis based on XRD clearly reveals two stages of development: dissolution of α-Si_3N_4 with the attendant formation of β-Si_3N_4; and the dissolution of β-Si_3N_4 with the attendant formation of β′-SiAlON of high Al/O compositions. A set of XRD patterns, taken from CY1, is shown in Fig. 2 to illustrate the development. Figure 2 shows the coexistence of α and β phases at 16 but not at 32 min, the progressive spread of β reflections toward lower angles from 32 to 128 min, and the very broad β′ reflections at 256 min. A relatively strong but diffuse background reflecting the glassy phase is also evident. The above features are generally representative of all four compositions at 1680°C.

The evolution of α/β-Si_3N_4 is confirmed using SEM back-scattering electron images. The images show a rapid decrease of the population of rounded α-Si_3N_4 crystals with time. After 32 min, only a trace amount of α-Si_3N_4 can be seen in samples CY2–CY4 but not in CY1. This suggests comparable kinetics in all the samples, with CY1 being somewhat faster. The SEM examination also determines that the crystal sizes are generally large enough (≥0.1 μm) at all times to produce sharp XRD reflections. Therefore, the broadening of reflections in Fig. 2 must be due to compositional spread and not small sizes. The β/β′ evolution is particularly pronounced at ~32.5°–33.5°, corresponding to $(10\bar{1}1)$ reflection. At 256 min, the broad reflections of β′-SiAlON are centered at locations that are consistent with $Si_2Al_4O_4N_4$.[13] The latter appears to be the equilibrium composition compatible with all the liquids used in our study.

(2) Volume Fraction of β/β′

The area fraction of β/β′ crystals measured by back-scattering SEM (e.g., Fig. 1(a)) is shown in Fig. 3 for all compositions. This

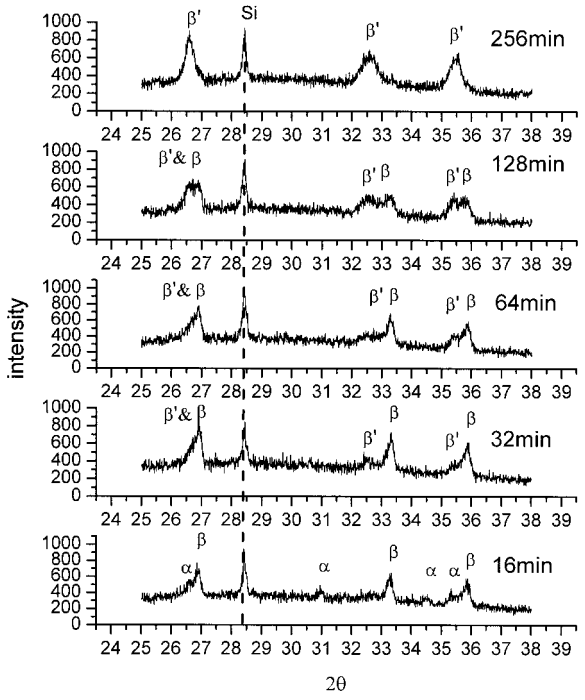

Fig. 2. XRD patterns of CY1 after various annealing times. Two phase transformations, from α to β and from β to β′, are shown. Silicon was added to the pulverized samples as internal standard. Background signal is due to glass matrix.

fraction is statistically the same as the volume fraction. The initial increase of the volume fraction with time is fast, as expected for α to β transformation. It later seems to saturate despite the progressive evolution to β′-SiAlON. This suggests that the main reaction in the latter evolution is Si-N/Al-O substitution, which entails little overall volume change, and not Al-O incorporation into the S-N matrix, which requires a very large volume increase.[14] The volume fractions, the initial value (taken at 8 min), and the final value (taken at 256 min) monotonically decrease from CY1 to CY4. Because the O/N and Al/Y/Mg ratios are the same for all samples, according to Table I, this decrease means that the composition range of the liquid is larger in the silicon-rich case and smaller in the (Mg,Y,Al)-rich case. This is consistent with our preliminary data that show the metastable β-Si_3N_4 solubility to increase from CY1 to CY4.

(3) Volume, Concentration, and Aspect Ratio of β/β′ Crystals

The average L and W of β/β′ crystals measured for each sample are presented below in the form of average (geometric mean)

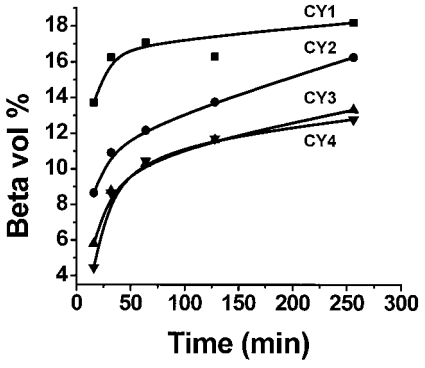

Fig. 3. Volume fraction of β/β′ phase increases over time for all compositions.

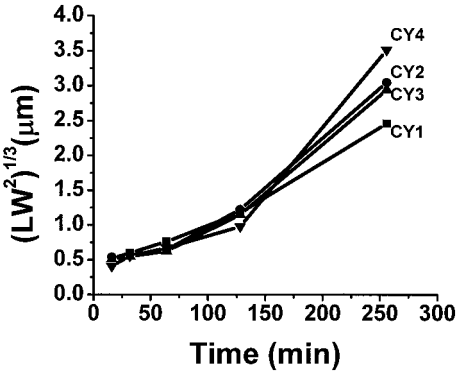

Fig. 4. Average linear dimension of β/β′ crystal increases with time for all compositions. This dimension is computed using geometric mean of length and squared width.

linear dimension $(LW^2)^{1/3}$ and aspect ratio (AR = L/W). (Their distributions are described and further analyzed in Part II.) As shown in Fig. 4, the average dimension remains relatively constant at shorter time, but it later increases by almost 1 order of magnitude at an accelerating rate. The same trend is observed in all four compositions. Because we already have obtained the volume fraction of β/β′ phases (Fig. 3), we can also calculate the volume concentration of β/β′ crystals by dividing the volume fraction by the average crystal volume ($0.75LW^2$). The results are shown in Fig. 5. In some samples (CY2 and CY3), we have found an initial increase in the crystal concentration from 16 to 32 min, which indicates additional nucleation during this period. Later, in all samples, the concentration decreases by almost 2 orders of magnitude from 64 to 256 min. Because the total volume of crystals changes very little during the latter period, the decrease in crystal concentration reflects the coarsening of average crystals, in agreement with Fig. 4. This overall trend thus follows the three general transformation stages: nucleation, growth, and coarsening, which correspond to, respectively, the stages of increasing, constant, and decreasing crystal concentrations.[15,16] To our knowledge, this is the first time that crystal concentration has been determined in Si_3N_4 systems.

The aspect ratios of β/β′ crystals are plotted in Fig. 6. The trends observed here are more complicated but nevertheless systematic. There is an initial increase of aspect ratio with time for all compositions; the duration of initial increase of aspect ratio increases from CY1 to CY4. Subsequently, there is a decrease of aspect ratio followed by the third stage during which the aspect ratio increases for CY1 but progressively changes to decreasing as the composition changes toward CY4. Except during brief periods of crossover, the aspect ratio systematically decreases from CY1 to CY4. On further examination of the data of length and width (see

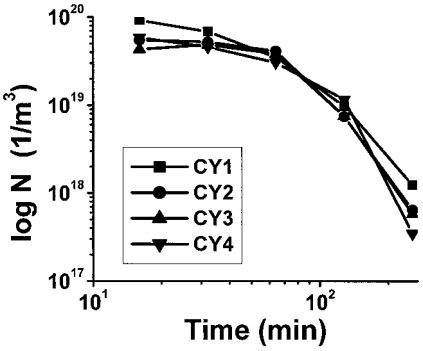

Fig. 5. Number of β/β′ crystals decreases rapidly after 64 min because of coarsening. For CY2 and CY3, the number initially increases slightly because of nucleation. Classical coarsening theories predict a 1/t dependence not obeyed here.

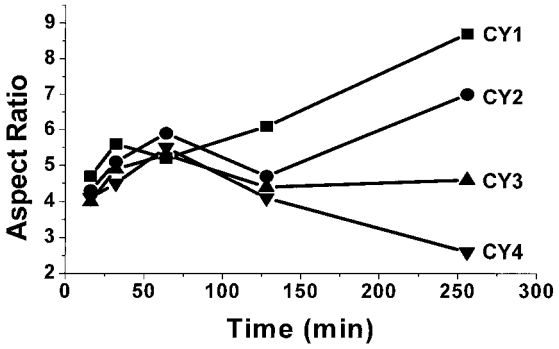

Fig. 6. Average aspect ratio of β/β′ crystal changes over time for compositions CY1 to CY4.

Figs. 3 and 6 of Part II), we find the initial increase of aspect ratio can be attributed to the length growth with minimum width growth, while the subsequent decrease of aspect ratio is associated with the onset of width growth. Later, the length growth reaccelerates; therefore, the aspect ratio begins to increase again, as in CY1 and CY2. However, in CY3 and, especially, CY4, the acceleration of width growth is relatively fast compared with length growth. Therefore, the aspect ratio continues to decrease, even at 256 min. These results show that, even in the coarsening stage, the aspect ratio can increase or decrease, depending on the composition. This is in contrast to the observation of decreasing aspect ratio in the coarsening stage, as reported by Krämer *et al*.,[5] based on the data of one (Si,Al,Y)(O,N) composition.

Selected examples of the microstructures are shown in Figs. 7 and 8 for two different times. These SEM micrographs and others not shown here confirm the observations above of volume growth and concentration decrease of β/β′ crystals. (Note the tenfold increase in the marker length from Fig. 7 to Fig. 8.) The lower aspect ratio of CY3 and CY4 compared with CY1 and CY2 at 256 min, due to larger width in Fig. 8, is also apparent.

IV. Discussion

(1) Nucleation Statistics of β-Si_3N_4

The data of the average volume and concentration of β crystals in the early stage of the transformation (up to 32 min) allow us to quantitatively assess the site statistics of β-Si_3N_4 nucleation. This is done by comparing the average dimensions and volume/weight fraction of α/β-Si_3N_4 crystals in the starting powders and those after substantial α-Si_3N_4 dissolution. This procedure is explained below, and a summary of the results is given in Table II.

First, we calculate the average density of the starting oxides and nitrides in the powders. This value varies from 3.47 to 3.39 Mg/m^3 from CY1 to CY4. Such values are 5%–10% higher than the density of Si_3N_4 (3.17 Mg/m^3). Second, the density of a crystal is typically 20% higher than that of a glass of the same composition. Therefore, the volume fraction of Si_3N_4 is estimated to be ~10%–15% lower than its weight fraction in the glass-ceramic. Because this difference is relatively small, we use weight fraction and volume fraction interchangeably without discrimination in the following discussion.

The comparison of crystal size and weight/volume fraction is shown in Table II. Here the dimension of the starting powder (50% of the size distribution) has been obtained from the manufacturer; the β fraction of the starting powder is the product of β content (<5%) and the weight percent of Si_3N_4 in the composition, and the data at 16 and 32 min are from Figs. 3 and 4. The sizes of β crystals at 16 and 32 min are similar to that of β crystals in the starting powder, but their volume/weight fractions exceed those of the starting β crystals by a factor of 5 to 20. This means that the number of β crystals has increased by a factor of 5 to 20. It is statistically unlikely that the β crystals in the starting powders are important in the nucleation statistics in our experiments.

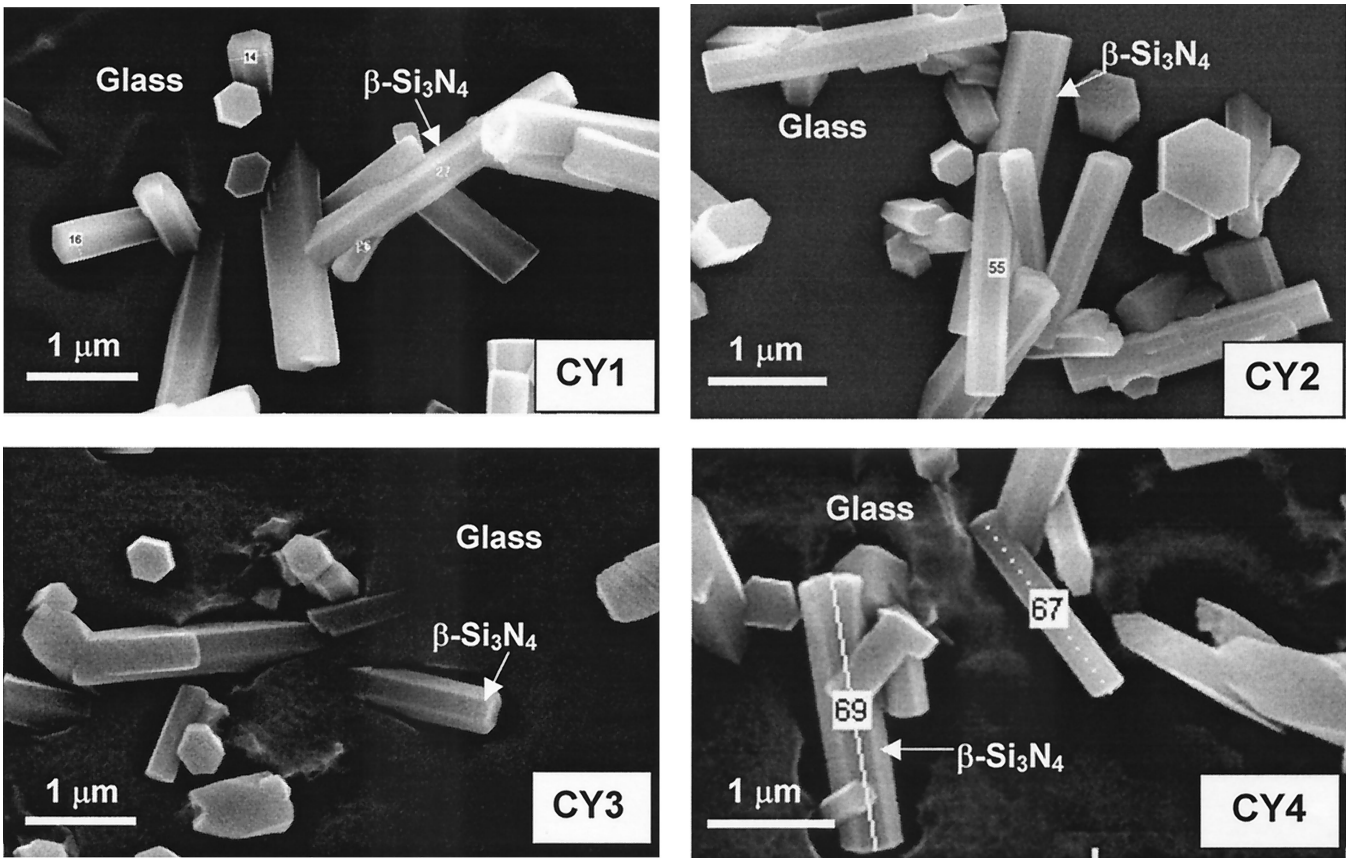

Fig. 7. Examples of morphologies of β/β′ crystals in various samples after 64 min at 1680°C. Numbered lines indicate length measurements on the original micrographs.

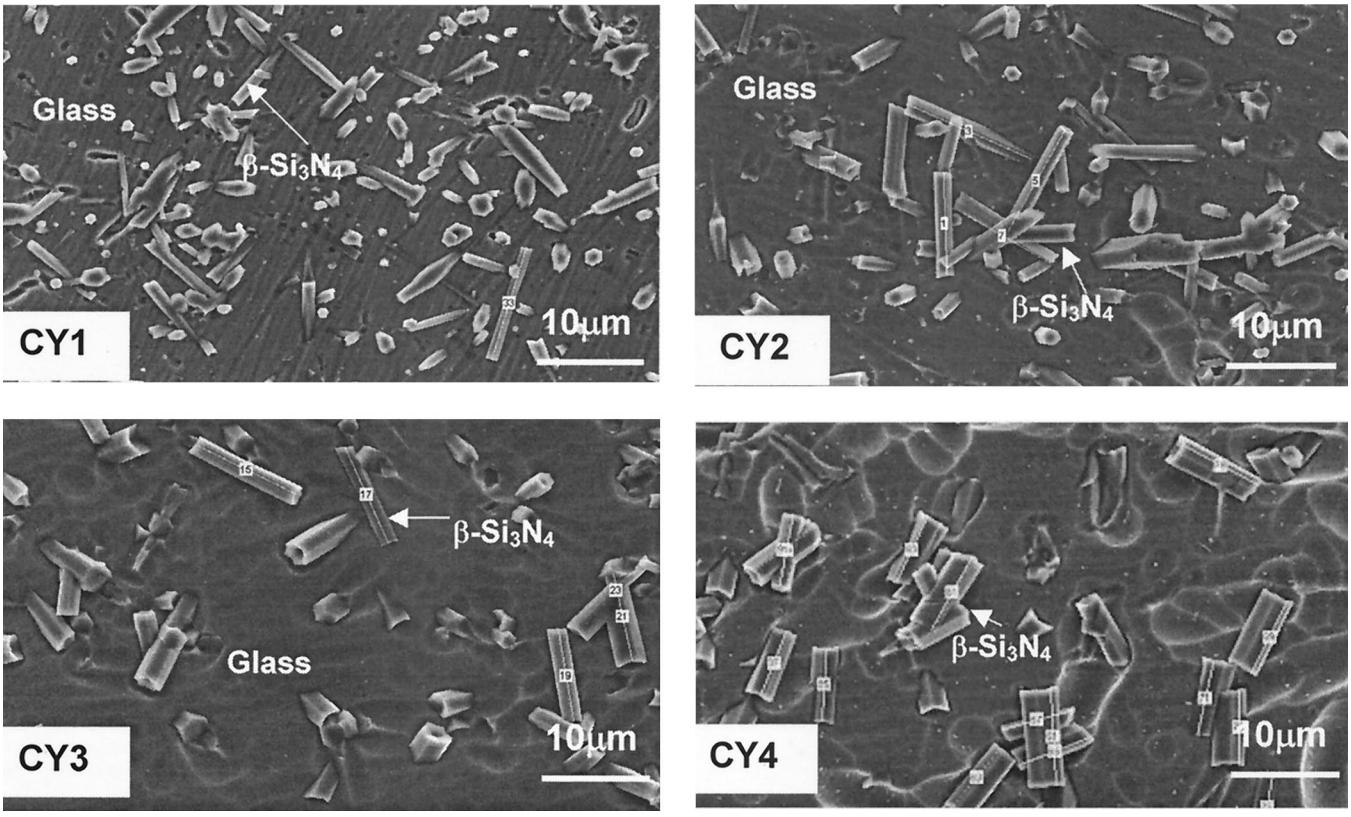

Fig. 8. Examples of morphologies of β/β′ crystals in various samples after 256 min at 1680°C. Numbered lines indicate length measurements on the original micrographs.

Direct evidence of β nucleation on α crystals is obtained by reviewing the microstructure at earlier times. Shown in Fig. 9 are three micrographs taken from CY1 after 8 min (Fig. 9(a)), after 16 min (Fig. 9(b)), and after 32 min (Fig. 9(c)). The evidence of the growth of small β crystals on α seeds is especially convincing in Figs. 9(a) and (b), which contain mushroomlike entities, where the stem is the β crystal. Many such features are found when we examine the crystal morphology in all compositions at 8 and 16 min. There have been previous reports of occasional β nucleation on α crystals, based on transmission electron microscopy (TEM) evidence.[17] The TEM evidence, however, can be fraught with poor sampling statistics. Therefore, the SEM micrographs here and the statistics shown in Table II offer the first definitive evidence that β nucleation on α crystals can be a common occurrence in Si_3N_4 systems.

The predominance of β nucleation on α seeds in our experiment is not likely to be related to the formation of β′-SiAlON, because, at 8 and 16 min, only β-Si_3N_4 precipitates. However, the above results are in apparent contradiction with the long-established understanding that β crystals in the starting powders control β nucleation during dissolution/reprecipitation.[18–20] The preference for β formation on β seeds is reasonable, because β-Si_3N_4 is identical in structure and composition to the reprecipitated phase. On the other hand, α-Si_3N_4 has essentially the same atomic structure on the basal plane as β-Si_3N_4. Therefore, heterogeneous nucleation of β-Si_3N_4 on the basal plane of α-Si_3N_4 also should be relatively favored, especially if the driving force for β-Si_3N_4 precipitation is large.

Table II. Particle Size and Fraction of β-Si_3N_4 Crystals in the Starting Powders and at Two Annealing Times during Precipitation

	Starting powder†		16 min anneal		32 min anneal	
Sample	Size (μm)‡	Fraction (vol%)	Size (μm)‡	Fraction (vol%)	Size (μm)‡	Fraction (vol%)
CY1	0.5	0.88	0.48	13.8	0.57	16.3
CY2	0.5	0.87	0.52	8.5	0.52	11.3
CY3	0.5	0.86	0.49	5.8	0.51	8.7
CY4	0.5	0.85	0.38	4.6	0.52	8.4

†Particle size of the starting powders is from manufacturer. ‡Particle size of the precipitates is calculated using the geometric mean $(LW^2)^{1/3}$.

According to Fig. 3, the volume fraction of β precipitates in CY1 reaches 0.16 after 32 min, when the composition of the crystals is still substantially the same as β-Si_3N_4. Comparing this value with the weight fraction (0.16) of α-Si_3N_4 in the starting powders, we can conclude that the solubility of β-Si_3N_4 in the liquid at this stage is rather low, of the order of 1%–2%. This value can be regarded as equilibrium solubility (C_o) in CY1. In our preliminary experiments, we have also established a metastable solubility (C) of α-Si_3N_4 in CY1 of ~11–12 wt%, below which there is no crystallization. Therefore, the supersaturation sustained by the liquid before β-Si_3N_4 in CY1 must be very large, of the order of several hundreds to thousands percent, resulting in a free energy ($kT \ln(C/C_o)$) of $\leq 10kT$ or ~1 eV at 1680°C. (Other compositions may have a smaller driving force because of higher metastable solubility of β-Si_3N_4, but the ratio of C/C_o is still substantial.) This very large driving force makes it possible to effect nucleation on the less potent sites, such as α-Si_3N_4 crystals. In contrast, in the case of liquid-phase sintering of Si_3N_4 ceramics, a much higher fraction (e.g., 0.8, compared with 0.15, as in our experiment) of Si_3N_4 is used. Therefore, the supersaturation is probably much smaller because of the presence of more plentiful (β seed) nucleation sites, which tend to facilitate early and easy nucleation that dissipates the driving force. This in turn precludes β nucleation on the less potent α seed, which is consistent with the literature of Si_3N_4 ceramics.

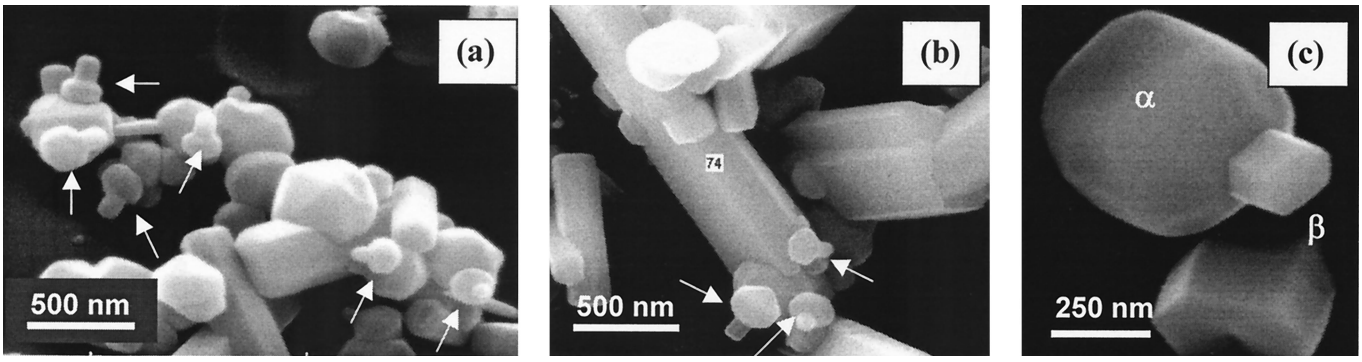

Fig. 9. Evidence of β crystals nucleating on α particle during α to β transformation in CY1 at (a) 8, (b) 16, and (c) 32 min, all at 1680°C. "Mushroom" feature showing β "stem" on α "cap" highlighted by arrows.

(2) Acid–Base Model for Aspect Ratio

The design of our experiments is to maintain an approximately constant liquid viscosity, hence, overall kinetics, by using the same O/N ratio and Al/Y/Mg ratio in all the samples. This design seems to be successful, judging from the similar transients for all samples in Figs. 3 and 5. Small differences in kinetics do exist. For example, CY1 (Fig. 2) seems to undergo the β to β′ conversion faster than other samples (not shown); however, the overall growth of crystal volume in CY1 is the slowest (Fig. 4). Overall, the main difference between different samples is mostly reflected in the evolution of the shape and aspect ratio of the crystals and not in the average kinetics. This makes it inappropriate to speculate the effect of liquid viscosity or any other average kinetic properties on the shape evolution observed in the present experiments.

There is a growing body of literature that suggests that the aspect ratios of Si_3N_4 and SiAlON crystals systematically correlate with the ionic radii of the network modifiers (M). Reports of the correlation have been recorded for dilute β′-SiAlON precipitates grown from liquids[20] and for dilute and concentrated α′-SiAlON crystals grown from liquids or in ceramics.[21] In all cases, the aspect ratio increases as the ionic radius increases. In the present study, although we did not vary the ionic radii of the network modifiers, a systematic variation of aspect ratio with composition and time was nevertheless observed because of the different Si/M ratio.

Interfacial segregation has been suggested as a possible mechanism that causes different aspect ratios.[20] In the following, we attempt to use the concept of an acid–base model to rationalize the tendency for segregation, which in turn may affect morphology development. The concept of acid–base has been used to rationalize the effect of network modifiers (yttrium and rare earths, as well as alkalines and alkaline earths) and network formers (silicon and aluminum) on wetting and reaction products of (Si,Al,M)(O,N) systems.[22] Here, the standard ranking of acidity by the field strength (z/r, where z is the formal charge of cation and r its radius) is followed, as shown in the lower part of Fig. 10. In this scale,

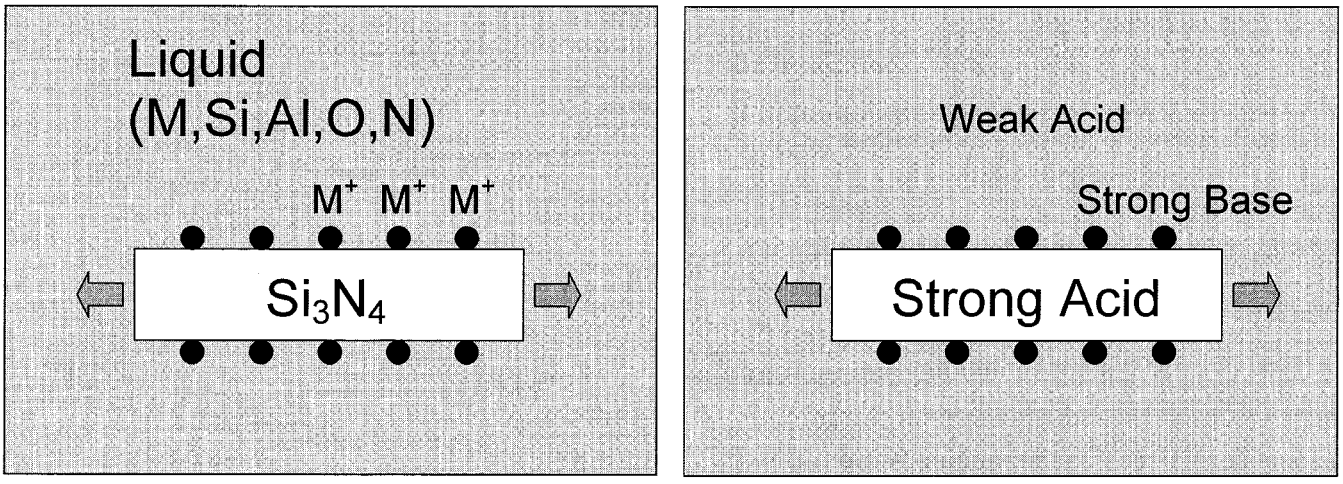

Acidity – z/r (field strength) after Ref. 21

	Si	Al	Yb	Y	Nd	La
z/r	15.4	7.7	3. 5	3.3	3.1	2.9

Acid → Base

Fig. 10. Estimation of acidity–basicity through field strength (lower table) and schematics for segregation of high basicity cations to the prismatic interfaces of high-acidity crystal (upper sketches). Field strength is calculated using cation change (z) in electronic units and ionic radius (r) in angstroms.

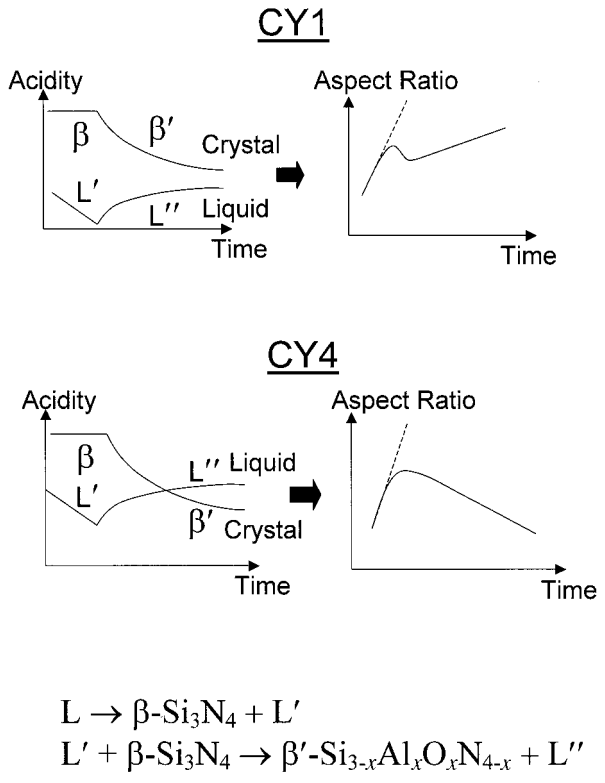

$$L \rightarrow \beta\text{-}Si_3N_4 + L'$$
$$L' + \beta\text{-}Si_3N_4 \rightarrow \beta'\text{-}Si_{3-x}Al_xO_xN_{4-x} + L''$$

Fig. 11. Schematic illustration of the acidity evolution in CY1 (upper part) and CY4 (lower part), following reactions shown at the bottom. Schematic aspect ratio whose change tracks the difference in acidity between crystal and liquid is shown on the right.

silicon is a strong acid, aluminum a weak acid, and yttrium and rare earths bases with the basicity increasing as the ionic size increases. Thermodynamic considerations then dictate that strong acids prefer to be associated (react) with strong bases, and weak acids with weak bases. (i.e., Ramberg's rule in crystal chemistry). To apply this concept to interfacial segregation, we consider the Si_3N_4 crystal as a strong acid, the (Si,Al,M)(O,N) liquid as a weak acid, and modifier cations as strong bases that tend to segregate to the prismatic faces of the crystal, as schematically illustrated in Fig. 10. Such tendency for segregation increases as the basicity of the segregating cation increases and as the acidity difference between the crystal and the liquid increases. It then follows that, as the ionic radius of M increases, for example, from ytterbium to lanthanum in the rare-earth series, segregation intensifies. If we further postulate that such strong segregation poisons the prismatic planes, causing them to grow much slower than the basal plane, then we expect an increase in the aspect ratio from ytterbium to lanthanum in the rare-earth series. Such a systematic correlation between the size of modifier cations and the aspect ratios has been observed for β-Si_3N_4, β′-SiAlON, and α′-SiAlON crystals.[20,21]

In the present study, the composition of modifying cations is fixed, but the Si/Al ratio increases from CY1 to CY4, suggesting increasing acidity of the liquid. In addition, as β-Si_3N_4 crystals precipitate and later convert, by Al-O/Si-N substitution, to β′-SiAlON (i.e., $Si_2Al_4O_4N_4$), the acidity of the liquid and the crystal undergo further changes. These changes in acidity of the crystal and the liquid are schematically illustrated on the left part of Fig. 11 for CY1 and CY4. The expected trend in aspect ratio is then determined by the difference in acidity between the crystal and the liquid, and the prediction is schematically plotted on the right part of Fig. 11, which is further discussed below.

Overall, the aspect ratio decreases from CY1 to CY4, because the acidity of the liquid increases, lowering the tendency for segregation. The strongest tendency for increasing segregation should happen during β-Si_3N_4 precipitation, because the crystal (containing only silicon and no aluminum) is most acidic at this point, and the liquid is becoming less acidic as it loses silicon to the crystal. This causes a rapid increase of aspect ratio at the early time. The trend is later reversed as β-Si_3N_4 converts to β′-SiAlON (e.g., $Si_2Al_4O_4N_4$), because the crystal (losing silicon and gaining aluminum) becomes less acidic, and the liquid (losing aluminum and gaining silicon) becomes more acidic. We then expect an increase of the prismatic growth rate. This causes the aspect ratio to either increase at a slower rate (as in CY1) or to decrease (as in CY4), depending on whether the ratio of the basal growth rate to prismatic growth rate is still higher or already lower than the aspect ratio at the time. These expected features are in qualitative agreement with the data of Fig. 6, suggesting the potential utility of acid–base concept.

(3) Overall Kinetics

The sequence of phase evolution, from α to β, then to β′, probably is adopted by the system to maximize nucleation advantage. Similar observations have been discussed in terms of coherent transformation in the Si_3N_4 literature.[17,23] The concept of coherent nucleation is based on the belief that a smaller misfit at the phase interface implies a lower interfacial energy and strain energy for the nucleus, thus, a smaller barrier for nucleation. This nucleation advantage often favors the precipitation of more coherent but less stable phases, before the precipitation of the less coherent but more stable phases (the classical example is the precipitation sequence in Al–Cu alloys[24]). In the present study, the same reasoning can rationalize the sequence of precipitation from the less stable β-Si_3N_4 to the more stable β′-SiAlON.

The advantage of early nucleation of β-Si_3N_4 is in its lattice parameters that are almost identical to those of α-Si_3N_4 at the (0001) interface. Therefore, coherent nucleation on these nuclei enjoys a low interfacial energy and little strain energy. In contrast, β′-SiAlON, which has the same structure as β-Si_3N_4 but larger lattice parameters, suffers a higher α/β′ interfacial energy and a larger strain energy when it nucleates on the α substrate. Later, after β precipitation is complete, the nucleation of thermodynamically more stable β′-SiAlON on the β crystals becomes more viable because of the similarity of their lattice structures. When the crystal exceeds a certain size, the strain energy due to the misfit between β and β′ also can be relieved by generating misfit dislocations on the interfaces. (Misfit dislocations between β and β′ have been previously observed using TEM.[17]) This size effect provides a possible explanation why a certain time (to achieve a certain size) must elapse before β′ precipitation is seen in our experiments.

The progression of β to β′ evolution is very slow and incomplete, even at the end of our experiments, as shown by the very broad XRD peaks of β′-SiAlON in Fig. 2 at 256 min. This is probably because, as new β′ precipitates onto existing β or β′, the latter composition becomes isolated from the liquid and, therefore, remains frozen unless the entire crystal later dissolves during microstructure coarsening. Such a long progression necessitates the consideration of β to β′ transformation in all the later kinetic stages in our experiments. Indeed, the simple picture of nucleation, α to β transformation, and coarsening is clearly inadequate, because the coarsening stage is apparently concomitant with β to β′ transformation in our experiment. (The β to β′ transformation cannot be identified with another growth stage, as in the case of α to β transformation, because the total crystal volume remains almost constant. This means that there is no new precipitation, only redistribution of matter between crystals.) Therefore, it is not surprising that features that fundamentally contradict the classical pictures of coarsening—such as the stronger than linear increase in crystal dimension in Fig. 4 (classical theory predicting a weaker than linear increase[8,9,16]) and the faster than $1/t$ (where t is the time) decrease in crystal concentration in Fig. 5 (classical theory predicting a $1/t$ dependence[8,9,16])—are seen. These aspects suggest an important influence of the β to β′ transformation on the kinetics and dynamics of crystal growth and coarsening, which are further explored in Part II.

V. Conclusions

(1) A range of glass compositions has been found that supports up to ~12% metastable Si_3N_4 without crystallization. Beyond this limit, most of the metastable Si_3N_4 precipitates under a very large driving force, making it possible to nucleate β-Si_3N_4 on α-Si_3N_4. Direct microscopic evidence and statistical data that support this conclusion are presented.

(2) In a nitrogen glass containing aluminum and oxygen, the initial precipitation of β-Si_3N_4 is followed by the conversion to β′-SiAlON. The conversion proceeds slowly and is not complete after 4 h at 1680°C in our experiments. It probably occurs by replacing Si-N by Al-O, in the process of particle dissolution and coarsening, and it involves relatively little volume change. This prolonged transformation has important effects on most aspects of crystal growth and coarsening in the (Si,Al,M)(O,N) systems.

(3) Crystal coarsening occurs in an accelerated manner, as evidenced by the time dependence of crystal concentration, which decreases much faster than the $1/t$ behavior expected for the classical coarsening phenomena.

(4) The evolution of aspect ratio strongly depends on the Si/(Al,Mg,Y) ratio. This is rationalized by the interfacial segregation of cations of high basicity. Because the degree of segregation tracks the difference in acidity–basicity of the liquid relative to the solid, the evolution of crystal and liquid compositions has a systematic effect on the aspect ratio.

Acknowledgment

This work was based on the Ph.D. dissertation of L.L.W. Helpful discussion with the members of the dissertation committee, Professor J. Halloran and Professor T. Pollock, is gratefully acknowledged.

References

[1]C. M. Hwang, T. Y. Tien, and I-W. Chen, "Anisotropic Grain Growth in Final Stage Sintering of Silicon Nitride Ceramics"; pp. 1034–39 in *Sintering '87, Proceedings of 4th International Symposium on Science and Technology of Sintering* , Vol. 2. (Nov. 4–7, 1987, Tokyo, Japan). Edited by S. Somiya, M. Shimada, M. Yoshimura, and R. Watanabe. Elsevier, New York, 1988.

[2]C. M. Hwang and T. Y. Tien, "Microstructure Development in Silicon Nitride Ceramics," *Mater. Sci. Forum*, **47**, 84–109 (1989).

[3]K.-R. Lai and T. Y. Tien, "Kinetics of β-Si_3N_4 Grain Growth in Si_3N_4 Ceramics Sintered under High Nitrogen Pressure," *J. Am. Ceram. Soc.*, **76** [1] 91–96 (1993).

[4]M. Krämer, M. J. Hoffmann, and G. Petzow, "Grain Growth Kinetics of Si_3N_4 during α/β-Transformation," *Acta Matall. Mater.*, **41** [10] 2939–47 (1993).

[5]M. Krämer, M. J. Hoffmann, and G. Petzow, "Grain Growth Studies of Silicon Nitride Dispersed in an Oxynitride Glass," *J. Am. Ceram. Soc.*, **76** [11] 2778–84 (1993).

[6]I-W. Chen and A. Rosenflanz, "A Tough SiAlON Ceramic Based on α-Si_3N_4 with a Whisker-Like Microstructure," *Nature (London)*, **389**, 701–704 (1997).

[7]D. P. Thompson, "Tough Cookery," *Nature (London)*, **389**, 675–77 (1997).

[8]I. M. Lifshitz and V. V. Slyozov, "The Kinetics of Precipitation from Supersaturated Solid Solutions," *J. Phys. Chem. Solids.*, **19** [1–2] 35–50 (1961).

[9]C. Wagner, "Theory of Precipitate Change by Redissolution," *Z. Electrochem.*, **65**, 581–91 (1961).

[10]A. J. Ardell, "The Effect of Volume Fraction on Particle Coarsening: Theoretical Considerations," *Acta Metall.*, **20** [1] 61–71 (1972).

[11]I-W. Chen, A. Davenport, and L.-L. Wang, "Accelerated Precipitate Coarsening due to a Concomitant Secondary Phase Transformation," *Acta Mater.*, **51** [6] 1691–703 (2003).

[12]L.-L. Wang, T.-Y. Tien, and I-W. Chen, "Morphology of Silicon Nitride Growth from a Liquid Phase," *J. Am. Ceram. Soc.*, **81** [10] 2677–86 (1998).

[13]C. P. Gazzara and D. R. Messier, "Determination of Phase Content of Si_3N_4 by X-ray Diffraction Analysis," *Am. Ceram. Soc. Bull.*, **56** [9] 777–80 (1977).

[14]K. H. Jack, "Review: Sialon and Related Nitrogen Ceramics," *J. Mater. Sci.*, **11**, 1135–58 (1976).

[15]S. Q. Xiao and P. Haasen, "HREM Investigation of Homogeneous Decomposition in a Ni–12 at.% Al Alloy," *Acta Metall. Mater.*, **39** [4] 651–59 (1991).

[16]R. Wagner, R. Kampmann, and P. W. Voorhees, "Homogeneous Second-Phase Precipitation"; p. 309–407 in *Phase Transformations in Materials*. Edited by G. Kostorz. Wiley–VCH, New York, 2001.

[17]S-L. Hwang and I-W. Chen, "Nucleation and Growth of β′-SiAlON," *J. Am. Ceram. Soc.*, **77** [7] 1719–28 (1994).

[18]F. F. Lange, "Fracture Toughness of Si_3N_4 as a Function of the Initial α-Phase Content," *J. Am. Ceram. Soc.*, **62** [7–8] 428–30 (1979).

[19]M. J. Hoffman and G. Petzow, "Microstructural Design of Si_3N_4 Ceramics"; pp. 3–14 in *Silicon Nitride Ceramics—Scientific and Technological Advances*, Materials Research Society Symposium Proceedings, Vol. 287. Edited by I-W. Chen *et al*. Materials Research Society, Pittsburgh, PA, 1993.

[20]M. J. Hoffmann, "Analysis of Microstructural Development and Mechanical Properties of Si_3N_4 Ceramics"; pp. 59–72 in *Tailoring of Mechanical Properties of Si_3N_4 Ceramics*. Edited by M. J. Hoffmann and G. Petzow. Kluwer, Dordrecht, The Netherlands, 1994.

[21]M. Y. Zenotchkine, R. A. Shuba, and I-W. Chen, "Effect of Seeding on the Microstructure and Mechanical Properties of α-SiAlON: III, Comparison of Modifying Cations," *J. Am. Ceram. Soc.*, **86** [7] 1168–75 (2003).

[22]M. Menon and I-W. Chen, "Reaction Densification of α′-SiAlON: I, Wetting Behavior and Acid–Base Reactions," *J. Am. Ceram. Soc.*, **78** [3] 545–52 (1995).

[23]A. Rosenflanz and I-W. Chen, "Kinetics of Phase Transformations in SiAlON Ceramics, II. Reaction Paths," *J. Eur. Ceram. Soc.*, **19**, 2337–48 (1999).

[24]D. A. Porter and K. E. Easterling, *Phase Transformations in Metal and Alloys*; pp. 291–301. Chapman and Hill, London, U.K. (printed by T. J. Press, Ltd., Padstow, Cornwall, U.K.), 1981. □